International Journal of Computational and Experimental Science and ENgineering (IJCESEN)

Vol. 12-No.1 (2026) pp. 447-461
http://www.ijcesen.com

ISSN: 2149-9144

Research Article

A Hybrid Monte Carlo–Machine Learning Framework for High-Energy Neutron Shielding Using Boron-Enhanced Concrete

Demet Sariyer[1]*, Elif Yıldırım[2]

[1]Manisa Celal Bayar University, Turgutlu Vocational High School, 45400, Turgutlu, Manisa, TURKEY
* **Corresponding Author Email:** demet.sariyer@cbu.edu.tr - **ORCID:** 0000-0002-7803-111X

[2] İstanbul Technical University, Faculty of Computer and Informatics Engineering, Computer Engineering Department, 34475, İstanbul, TURKEY
Email: elifyildirim@itu.edu.tr - **ORCID:** 0000-0002-1599-9473

Article Info:

DOI: 10.22399/ijcesen.4827
Received : 18 November 2025
Revised : 11 January 2026
Accepted : 17 January 2026

Keywords

High-energy neutron shielding,
Boron-enhanced concrete
Monte Carlo simulation
Machine learning
Surrogate modeling

Abstract:

Secondary neutrons produced by proton-target interactions in high-energy proton accelerator facilities present a major shielding challenge due to their high penetrability and broad energy spectra. In this study, neutron dose attenuation in B_4C- and FeB-enhanced concretes containing 5%, 10%, and 15% additives was investigated at a proton energy of 1000 MeV using FLUKA-based Monte Carlo (MC) simulations coupled with Machine-learning (ML) surrogate models.MC-generated dose data were used to train log-linear Linear Regression (log-linear LR), K-Nearest Neighbors (KNN), Random Forest (RF), and Gradient Boosting Regressor (GBR) models to enable rapid dose prediction. The results show that RF and GBR achieve the highest predictive accuracy under all configurations, with test-set R^2 values of approximately 0.98-0.99 in tunnel air and 0.99-0.996 in concrete shielding. In contrast, the LR model performs poorly in shielding regions due to strong nonlinearity, while KNN also provides high predictive accuracy exceeding 90%, albeit with lower performance compared to RF and GBR. A comparative analysis reveals that FeB-enhanced concrete exhibits more complex attenuation behavior due to the combined effects of iron-induced scattering and boron absorption. Overall, the validated hybrid MC-ML framework demonstrates that RF- and GBR-based surrogate models provide a fast, reliable, and computationally efficient approach for neutron dose estimation and shielding optimization in high-energy proton accelerator facilities.

1. Introduction

The steadily increasing use of ionizing radiation in nuclear facilities, medical applications, and industrial systems necessitates the development of effective, reliable, and sustainable shielding solutions against these radiation types. In particular, the high dose levels encountered in particle accelerators, research reactors, and radiation-producing industrial facilities render shielding design one of the most critical components of facility safety. In this context, concrete stands out as one of the most widely used construction materials for radiation shielding owing to its high mechanical strength, cost-effectiveness, wide availability, and the possibility of tailoring its properties through the incorporation of various additives [1-3]. The radiation shielding performance of concrete is governed by the interaction mechanisms of gamma rays and neutrons within the material. For gamma radiation, concrete density and effective atomic number are among the primary determining factors, whereas neutron shielding represents a more complex process that requires the joint optimization of moderation and absorption mechanisms. The concrete matrix, due to its hydrogen content, acts as an effective moderator for fast neutrons; however, a shielding strategy based solely on moderation is insufficient, particularly in high-energy neutron fields [4-6].

In high-energy proton accelerators, especially under proton–target interactions at energies on the order of 1000 MeV, secondary neutrons produced over a broad energy spectrum pose a significant engineering challenge in shielding design because of their high penetration capability. Compared to

thermal or low-energy neutrons, these high-energy neutrons penetrate much deeper into shielding materials, often necessitating very thick shielding structures to achieve effective attenuation. Numerous studies have reported that, in shielding systems relying solely on standard concrete, the required thicknesses may exceed practical and economic limits. This issue further complicates shielding design in tunnel-type accelerator facilities, where spatial, economic, and structural constraints are particularly restrictive [7-13].

In response to these challenges, recent years have witnessed growing interest in additive-enhanced concrete approaches aimed at improving shielding performance. While heavy aggregates such as barite, hematite, and magnetite are effective in enhancing gamma-ray shielding, the incorporation of boron-based additives into concrete has emerged as a promising strategy for neutron shielding. Compared to standard concrete, additive-enhanced concrete systems provide higher attenuation efficiency, enabling a reduction in the required shielding thickness and facilitating more compact shielding designs [5-9, 10,12].

Within this framework, concretes incorporating boron carbide (B_4C) and ferroboron-based additives have attracted particular attention for high-energy neutron shielding applications. B_4C supports the efficient absorption of moderated neutrons owing to its high neutron capture cross-section, while ferroboron (FeB, Fe_2B) additives offer a synergistic shielding mechanism by combining the scattering properties of iron with the absorption capability of boron. The combined action of neutron moderation provided by the concrete matrix and neutron absorption induced by boron-based additives constitutes a critical advantage in attenuating secondary neutrons generated in high-energy proton accelerators. As a result, overall neutron dose levels can be reduced while simultaneously optimizing shielding thickness [1,6-10,12,14].

In the literature, in addition to comprehensive review and experimental studies on concrete-based radiation shielding, several investigations have addressed the neutron shielding performance of B_4C- and ferroboron-enhanced concretes. Studies conducted by Sarıyer *et al.* and other researchers have demonstrated that additive-enhanced concrete systems offer significant advantages over standard concrete in reducing neutron dose. Nevertheless, a substantial portion of existing studies has focused on low- and intermediate-energy neutron fields or specific geometric configurations. Consequently, systematic and direct comparisons of the performance of B_4C- and ferroboron-enhanced concretes under identical geometric and physical conditions in high-energy neutron fields remain limited in the literature [1,6-10,12,14].

Most studies on high-energy neutron shielding rely on Monte Carlo (MC)-based simulation codes, which can model radiation transport processes in a detailed and physically accurate manner [1,3,4,7-14]. Although MC methods can represent the behavior of secondary neutrons generated by proton–target interactions with high fidelity, their computational cost—particularly for accelerator applications at energies around 1000 MeV—significantly limits extensive parameter space exploration, multi-scenario analyses, and rapid optimization studies. Consequently, in recent years, the integration of high-dimensional datasets generated by MC simulations with machine learning (ML)–based surrogate models has emerged as a complementary approach to alleviate computational burdens [15,16].

ML is a data-driven approach that aims to predict complex and nonlinear system behavior by automatically learning patterns and relationships from data, offering significant advantages in multi-parameter problems where classical deterministic or analytical methods are inadequate. In computationally intensive applications such as radiation shielding-where geometry, material composition, energy, and interaction processes jointly influence system behavior-ML enables the development of low-fidelity surrogate models that learn from high-dimensional datasets generated by physics-based MC simulations and provide rapid, low-cost predictions. The primary objective of such ML-based models is not to replace high-fidelity calculations, but rather to deliver reasonably accurate estimates that support rapid preliminary assessments, parameter screening, design optimization, and uncertainty analysis. Their most notable advantages include low computational cost, limited resource requirements, and the ability to explore large parameter spaces efficiently. Nevertheless, it must be emphasized that ML approaches do not explicitly represent the underlying physical processes and therefore cannot substitute physics-based MC simulations. From the perspective of reliable and practical shielding design, the critical framework is a validation-driven hybrid (MC–ML) approach, in which ML-based predictions are systematically verified against high-accuracy MC calculations before being used in final design decisions. In this way, ML accelerates the design process, while MC methods ensure the necessary physical accuracy and reliability [15-24].

Within this context, the literature contains a limited but noteworthy number of studies based on MC-ML integration. Chen *et al.* (2023) simulated 200 shielding configurations using MCNP to optimize

neutron beam shutters in a cyclotron-based neutron production system; using the resulting data, they trained a fully connected artificial neural network (ANN), applied it to 1,000 randomly generated shielding structures, and subsequently validated the top 20 configurations with MCNP. This approach demonstrated that ML-based methods can jointly achieve accuracy and computational efficiency in neutron shielding optimization [17]. Edelen *et al.* (2016) investigated the contribution of ANN-based methods to modeling nonlinear and complex processes in particle accelerator control systems, showing—through an experimental ANN-assisted resonance control application at FAST/Fermilab—that classical control approaches are insufficient due to multi-subsystem interactions and long-term stability requirements, whereas ANN-based techniques provide substantial benefits in predicting system dynamics and enabling adaptive control [22]. Rajarshi Pal Chowdhury *et al.* (2023) developed a 1D-CNN capable of rapidly predicting differential neutron flux to reduce the high computational cost of PHITS-based MC calculations in the FRIB case; they reported that the model, trained over the 1–250 MeV energy range, could reproduce neutron spectra with approximately 10% error in tests involving 10,000 samples, achieving millisecond-level prediction times and successful effective dose estimation [19]. In a subsequent study, Pal Chowdhury *et al.* (2026) demonstrated that a CNN-based surrogate model emulating MC transport simulations could learn neutron attenuation behavior under varying energy and material conditions and predict post-shield neutron flux almost instantaneously with reasonable accuracy; the applicability of the approach was highlighted in the context of effective dose rate calculations and shielding optimization for FRIB applications [23]. Overall, these studies indicate that MC-ML hybrid approaches provide an advantageous framework for rapid exploration of the design space and multi-parameter optimization in radiation shielding design for accelerator facilities [17,22-24].

The aim of the present study is to develop a comprehensive shielding model that integrates FLUKA-based MC simulations with ML techniques for the effective attenuation of secondary neutron radiation generated under abnormal operating conditions in high-energy proton accelerators. Within this scope, dose prediction models were constructed for various medium-shield configurations at an energy level of 1000 MeV using logarithmic linear regression [25-29], Gradient Boosting Regressor [27,30-34], K-Nearest Neighbors (KNN) regression [30,31,35,36], and Random Forest algorithms [27,30,31,37], and their predictive performances were systematically evaluated through a comparative approach. Furthermore, the hybrid MC-ML methodology—addressed in a limited number of studies in the literature—was examined in detail, and the findings were shown to provide original and meaningful contributions toward the optimization of radiation shielding design.

2. Material and Methods

In this study, dose distributions of secondary neutrons generated by the interaction of 1000 MeV protons with the target material were investigated in detail within the air-filled tunnel and along the surrounding concrete shielding layers containing B_4C and FeB additives at different concentrations (5%, 10%, and 15%). The shielding analyses were carried out using versions 2011.2b and 2011.2c of the FLUKA MC simulation code, and dose values corresponding to various shielding thicknesses and radial distances were calculated for each shielding configuration. The simulation outputs obtained were subsequently used for the development and performance evaluation of regression-based machine learning algorithms. During this process, data preprocessing, model training, and performance analysis were conducted using the Python programming language, with extensive use of open-source data science libraries including NumPy, Pandas, Matplotlib, and Scikit-learn.

2.1 FLUKA-Based Simulation Design and Data Generation

To accurately model particle–matter interactions, a spherical geometry with a radius of 25 m was constructed using the FLUKA MC simulation code. The outermost region of the sphere was defined as a 1 m thick *blackhole* layer to terminate particle

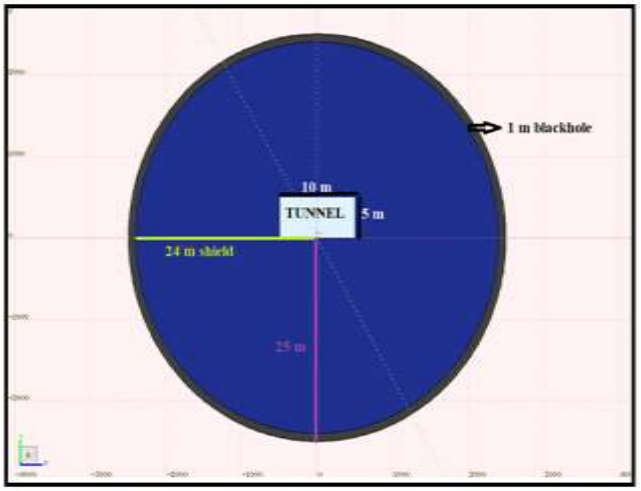

Figure 1. *Computational geometry of the tunnel and surrounding concrete shielding modeled in the FLUKA MC simulations*

tracking. Within the sphere, a shielding region with a total thickness of 24 m was modelled and separately applied for concrete shielding materials containing B_4C and FeB additives at concentrations of 5%, 10%, and 15%. At the center of the spherical geometry, an air-filled tunnel with dimensions of 5 m (x-axis) × 5 m (y-axis) × 10 m (z-axis) was placed. The computational geometry used in this study is schematically illustrated in Figure 1.It is well known that protons propagating along accelerator tunnels interact with copper surfaces, which are widely used in the internal structures of accelerator components such as quadrupole magnets and RF cavities, particularly in regions where beam losses occur. For this reason, a cubic copper block with dimensions of 5 cm × 5 cm × 5 cm and parallel faces was selected as the target material. The chosen copper target with a thickness of 5 cm was not designed to completely stop 1000 MeV protons, since at this energy level the proton range in copper extends to several tens of centimetres. Instead, the copper target was modelled to represent localized proton–material interactions occurring on copper components under realistic beam loss conditions, as well as the subsequent production of secondary particles, primarily neutrons. Accordingly, the copper target was treated not as a full proton absorber but as a partial interaction region.

To model the proton source in a manner that enables the formation of maximum dose in all directions, a point-like proton source was defined with reference to the exact geometric center of the copper target. This definition does not imply that protons are physically generated within the target volume; rather, it represents an idealized approach to beam-material interactions in accelerator components. To prevent direct activation of the shielding materials by the primary proton beam, the beam axis was positioned 2.5 m away from the tunnel side walls and 4 m below the tunnel ceiling. The location of the copper target within the air-filled tunnel, together with the reference point of the proton source and the relative placement of the beam axis, is schematically illustrated in Figure 2. When MC-based methods are employed in shielding design calculations, the reliability of the results decreases significantly due to increased statistical uncertainties, particularly in simulations performed with a limited number of particles. Therefore, in order to ensure the statistical accuracy required by the MC approach, five independent simulation cycles were carried out in this study, each involving 6×10^8 primary particles and using different random number seeds. In general, MC simulations that involve high-energy particle transport and the tracking of a large number of events are known to entail extremely high computational costs and long execution times on

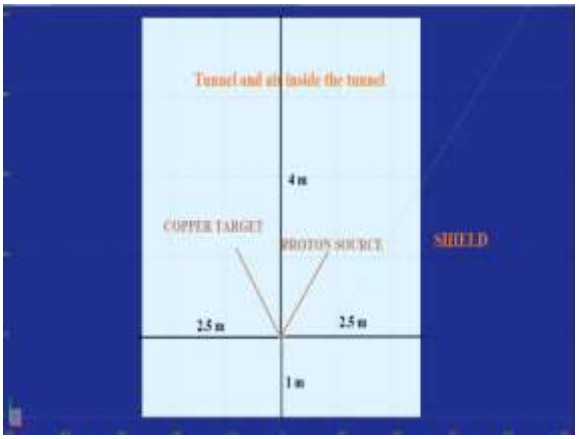

Figure 2. *Schematic representation of the proton source and copper target placement inside the tunnel relative to the surrounding shielding.*

conventional desktop computers. Consequently, the use of high-performance computing (HPC) cluster infrastructures becomes indispensable for such calculations. Accordingly, all MC simulations presented in this study were performed on the TR-Grid high-performance computing cluster.

The outputs obtained from the simulations were analyzed in detail based on the data files generated by the FLUKA code. To quantitatively determine dose distributions at different spatial locations along the tunnel, the three-dimensional spatial scoring detector of FLUKA, namely the USRBIN card, was employed. The detector volume was defined as 3400 cm, 3000 cm, and 1900 cm along the x-, y-, and z-axes, respectively, with the corresponding numbers of bins set to 340, 300, and 190. As a result of this configuration, the spatial resolution of the detector system used in the simulations was set to unit elements (voxels) with dimensions of 10 × 10 × 10 cm^3.

The dose distributions calculated for 1000 MeV protons were visualized using FLAIR, the graphical user interface of FLUKA, and comprehensive quantitative analyses were performed on the resulting data.

2.2. Selection and Training of Machine Learning Models

ML is a data-driven approach that enables a computer system to automatically discover patterns and statistical relationships within given datasets and to generate generalizable inferences from these relationships. The ML process fundamentally consists of two main stages. The first stage is the training phase, during which the model learns the input–output relationships present in the data. This is followed by the testing and validation phase, in which the predictive accuracy and generalization capability of the trained model are evaluated. The

testing process should not be regarded as a decision-making mechanism, but rather as a validation tool used to assess the reliability and predictive performance of the model. If the validation results are found to be inadequate, the model parameters are updated and the training process is repeated. Final prediction or decision generation is performed only after the model has successfully completed the validation stage. Throughout this process, two distinct datasets are employed for performance evaluation: a training dataset used during the learning phase and a test dataset consisting of samples previously unseen by the model. While the training dataset is utilized for learning, including data preprocessing and feature extraction, the test dataset is used to quantitatively assess the model's generalization ability. Model performance is determined using numerical metrics by comparing predictions generated on the test dataset with corresponding reference values [30].

ML methods are generally classified into three main learning paradigms: supervised learning, unsupervised learning, and reinforcement learning [38,39]. Supervised learning encompasses methods in which the output is predefined during the prediction or decision-making process and the model learns input-output relationships accordingly. Supervised learning approaches are widely used, particularly for classification and regression problems.

In this study, regression-based ML models were developed to predict neutron dose distributions under a 1000 MeV energy level for concrete-air and concrete-shield configurations containing B_4C and FeB additives at concentrations of 5%, 10%, and 15%, using data obtained from FLUKA MC simulations. The problem was formulated as a regression task aimed at predicting neutron dose, which is a continuous physical quantity. The target variable represents dose values calculated at different lateral distances from the beam source, while the model inputs consist of the corresponding lateral distance values. The analyses indicate that the dose decreases monotonically with increasing lateral distance and that this behaviour can be described as a combination of an inverse-square law component and multiple exponential attenuation mechanisms. In this context, the primary objective of the model is to accurately predict the spatial distribution of dose along different lateral positions. Accordingly, regression-based approaches capable of learning the functional relationship between a continuous dependent variable and an independent variable provide a suitable framework for this problem.

The regression models employed in this study were selected through a deliberate and comparative process, taking into account both the physical nature and the statistical characteristics of the radiation shielding problem. Since the distance-dependent attenuation behaviour of neutron dose exhibits nonlinear, multi-scale, and physically complex characteristics, the selected models were required to capture both the dominant physical trends, and the complex nonlinear relationships present in the data. To this end, Logarithmic Linear Regression (log-linear LR) was employed as a reference (baseline) model to represent the dominant physical trend of the dose-distance relationship. This baseline model enables a quantitative assessment of the performance gains achieved by more advanced ML methods. Gradient Boosting Regressor (GBR) and Random Forest (RF) algorithms were selected due to their strong capability to model nonlinear attenuation behaviour and complex spatial relationships commonly encountered in radiation transport problems. Owing to their decision tree–based ensemble structures, these methods can effectively learn dominant physical patterns across different distance regimes while maintaining high generalization performance. The K-Nearest Neighbors (KNN) regressor was included as an intuitive, non-parametric comparison model based on local neighborhood relationships. Its lack of strong parametric assumptions makes KNN particularly suitable for analysing local variations in dose distributions that exhibit smooth and monotonic behaviour. The selected model set spans a broad methodological range, from simple linear approaches to advanced ensemble-based methods, allowing for a comprehensive comparative evaluation of the predictive capabilities of ML-based surrogate models for radiation shielding applications.

The dataset used in this study consists of independent samples obtained from FLUKA MC radiation transport simulations. Each data point represents a radiation transport output calculated for a specific proton energy, environmental/shielding configuration, and radial distance. This approach enables systematic sampling of radiation fields under different physical scenarios. The input parameters provided to the ML models include the lateral distance variable x (cm), representing different radial distances within the air-filled tunnel and varying shielding thicknesses within the shielding region, as well as proton energy levels. In this way, the models are trained to learn the spatial variation of radiation fields both in air and within shielding materials. The output data consist of the corresponding dose equivalent values, H (μSv/h), calculated under the same physical conditions.

The dataset constructed in this study comprises a total of 1081 data points, obtained from calculations performed in air and shielding regions for different

energy levels and shielding configurations. Each data point is defined as an input–output pair representing a specific physical scenario and is treated as an independent sample during the training and testing of the ML models. The dataset was divided into separate subsets for each environmental and shielding configuration, and these subsets were further structured into training and test datasets. To ensure an appropriate bias-variance balance and to reduce the risk of overfitting or underfitting, 75% of the dataset was used for training and 25% for testing. This split ratio is widely adopted in the literature and has been shown to provide reliable performance assessment [40].

The test dataset consists of samples not encountered during the training phase and is used to evaluate the generalization capability of the models after training is completed. This approach allows model performance to be validated on an independent dataset not involved in the learning process, thereby enabling the identification of potential overfitting (bias) or underfitting (variance) issues. The convergence of training and validation errors to similar values indicates that the model has been sufficiently optimized and does not require further training [24].

Model performance was evaluated using the coefficient of determination (R^2) and the root mean square error (RMSE) metrics. The target variable was defined as neutron dose, H (μSv/h), while the input variables were specified as the lateral distance within the tunnel, x (cm), and the proton energy level, E (MeV). Each environmental and shielding configuration was modelled separately, and all regression algorithms were applied within a comparative framework.

3. Results and Discussions

This study was conducted to provide a scientific contribution to shielding design for radiation safety in proton accelerator facilities. The primary objective of the study is to rapidly predict neutron doses at different distances along the accelerator tunnel under abnormal operating conditions using ML-based models.

The ML-based dose predictions developed in this work were compared with results obtained from FLUKA-based MC simulations performed at an energy level of 1000 MeV in order to assess their accuracy. The dataset consisting of a total of 1081 data points used for training and testing the ML models was not intended to replace high-fidelity MC simulations; rather, it was employed to construct surrogate models that enable rapid preliminary assessment, parameter screening, and early-stage design support prior to detailed shielding calculations. Through this approach, reasonably accurate dose predictions can be obtained with low computational cost during the early phases of the shielding design process, while final design decisions remain grounded in physics-based MC simulations.

The dose distributions of secondary neutrons produced by the interaction of 1000 MeV protons with a copper target were used to train and test log-linear LR, GBR, KNN, and RF models for each material-environment configuration. For each configuration, graphical comparisons between the predicted and observed dose values are presented separately.

Figure 3 shows the dose distribution profiles obtained in an air environment at the 1000 MeV energy level: (a) concrete containing 5% B_4C-air, (b) concrete containing 10% B_4C-air, and (c) concrete containing 15% B_4C-air. Figure 4 presents the dose distribution profiles obtained in a shielded environment at the same energy level: (a) concrete containing 5% B_4C-shield, (b) concrete containing 10% B_4C-shield, and (c) concrete containing 15% B_4C-shield. Similarly, Figure 5 shows the dose distribution profiles obtained in an air environment at the 1000 MeV energy level: (a) concrete containing 5% FeB-air, (b) concrete containing 10% FeB-air, and (c) concrete containing 15% FeB-air. Figure 6 presents the dose distribution profiles obtained in a shielded environment at the same energy level: (a) concrete containing 5% FeB-shield, (b) concrete containing 10% FeB-shield, and (c) concrete containing 15% FeB-shield.

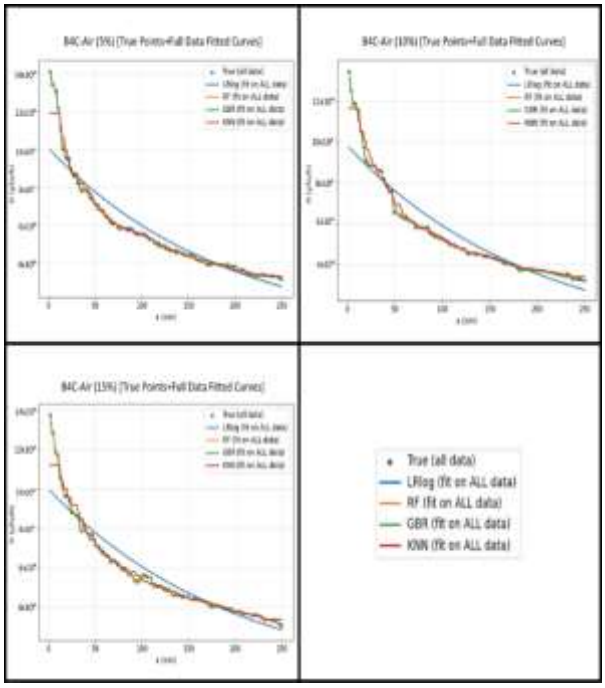

Figure 3. *True dose measurements and full-data fitted regression curves for* ***B_4C*** *in air at boron fractions of 5%, 10%, and 15%*

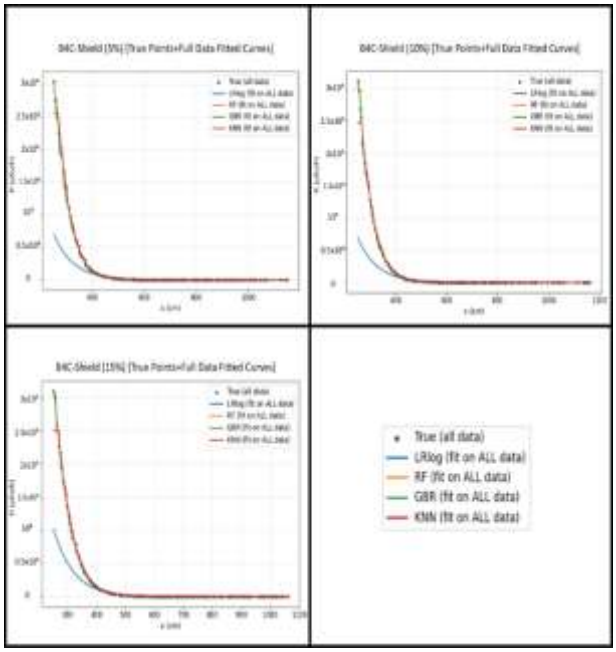

Figure 4. *True dose measurements and full-data fitted regression curves for* ***B_4C*** *in shield at boron fractions of 5%, 10%, and 15%*

The dose distribution profiles presented in Figures 3 and 4 reveal a clear distinction between neutron transport behavior in the tunnel air environment and within the concrete shielding for B_4C-enhanced concrete. In the tunnel air environment, the dose decreases smoothly and monotonically with increasing distance from the source, whereas within the concrete shielding the dose is reduced by several orders of magnitude over much shorter distances, exhibiting a steep, highly nonlinear attenuation profile. This contrast reflects the dominant physical mechanisms in each medium: geometric spreading and scattering prevail in air, while neutron moderation and absorption govern the attenuation process within the concrete shield.A comparative assessment of the regression curves clearly demonstrates the superiority of nonlinear modeling approaches. The Random Forest (RF) and Gradient Boosting Regressor (GBR) models consistently reproduce the reference dose values with high fidelity in both environments. These models accurately capture the steep dose gradients in the vicinity of the source as well as the more gradual attenuation behavior observed at larger distances, yielding physically consistent predictions across the entire spatial range. Their near coincidence with the true dose points in the shielding environment highlights their ability to represent the multi-scale and strongly nonlinear nature of neutron attenuation in B_4C-enhanced concrete.

The K-Nearest Neighbors (KNN) model, while capable of following the general attenuation trend in the tunnel air environment, exhibits local fluctuations and reduced stability, particularly at intermediate distances. Its performance deteriorates more noticeably within the concrete shielding, where rapid dose reductions occur. In these high-gradient regions, KNN predictions deviate from the reference data, indicating that its locally driven, instance-based structure is not well suited to capturing the complex and rapidly varying physical processes governing neutron transport in shielding materials.

The log-linear Linear Regression (LR) model performs inadequately in both environments, failing to represent the inherently nonlinear dose–distance relationship. This limitation is especially evident within the concrete shielding, where the sharp dose attenuation cannot be reproduced by a log-linear formulation, leading to substantial deviations from the true dose distribution. These observations underscore the inability of simple linear approaches to describe neutron transport phenomena in high-energy accelerator shielding problems.Overall, the results presented in Figures 3 and 4 demonstrate that Random Forest and Gradient Boosting Regressor models provide the most reliable and physically meaningful predictions of secondary neutron dose distributions for B_4C-enhanced concrete. Their robust performance in both tunnel air and concrete shielding environments confirms their suitability for modeling complex, nonlinear neutron attenuation behavior. In contrast, KNN offers only limited applicability, and linear regression approaches prove inadequate for accurately representing the physics of neutron shielding in high-energy proton accelerator facilities. The dose distribution profiles presented in Figures 5 and 6 demonstrate a clear distinction in neutron transport behavior between the tunnel air

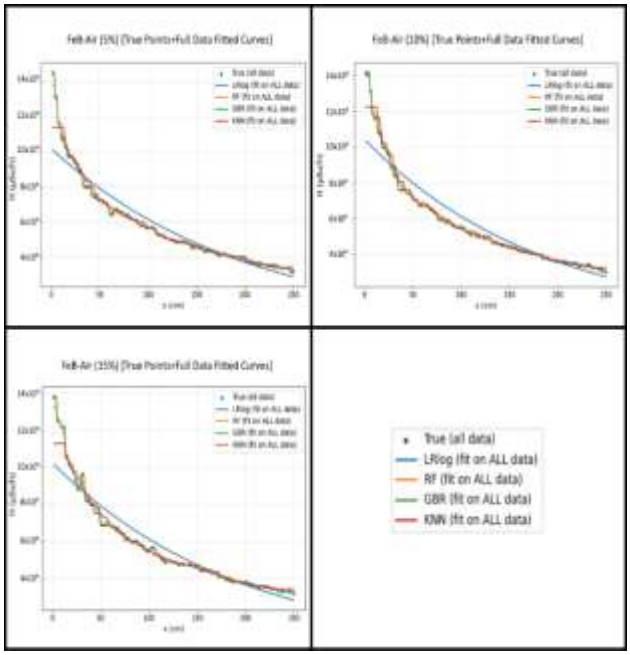

Figure 5. *True dose measurements and full-data fitted regression curves for* ***FeB*** *in air at boron fractions of 5%, 10%, and 15%*

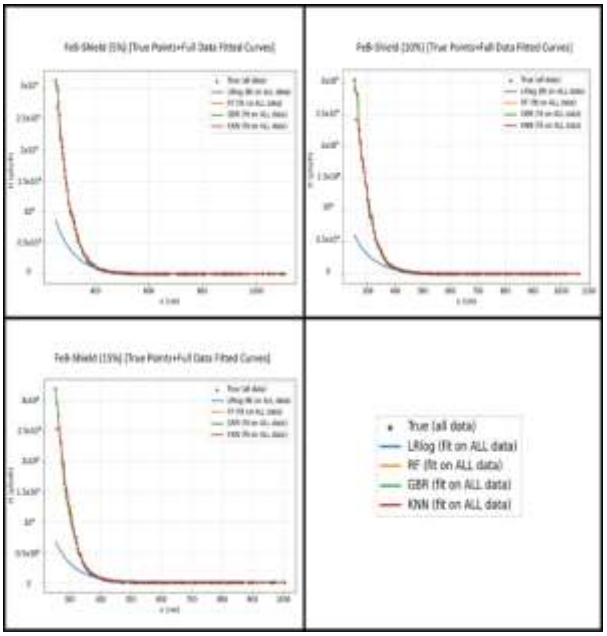

Figure 6. *True dose measurements and full-data fitted regression curves for FeB in shield at boron fractions of 5%, 10%, and 15%*

environment and the concrete shielding for FeB-enhanced concrete. In the tunnel air environment, the dose decreases smoothly and monotonically with increasing distance from the source, whereas within the concrete shielding the dose is reduced by several orders of magnitude over much shorter distances, exhibiting a steep and strongly nonlinear attenuation profile. This contrast reflects the change in dominant physical mechanisms: geometric spreading and scattering govern neutron transport in air, while moderation, scattering, and absorption processes collectively control dose attenuation within the concrete shield.An examination of Figure 5, corresponding to the tunnel air environment, shows that for all FeB fractions (5%, 10%, and 15%) the dose decreases regularly with distance. A comparison of the regression curves highlights the superiority of nonlinear modeling approaches. The RF and GBR models accurately reproduce the true dose values across the entire spatial range, capturing both the high dose gradients near the source and the more gradual attenuation behavior observed at larger distances. In contrast, the KNN model follows the general trend but exhibits local fluctuations and reduced stability, particularly at intermediate distances. The log-linear LR model performs inadequately even in the air environment, failing to represent the nonlinear dose-distance relationship and showing systematic deviations at medium and long distances.The dose distributions within the concrete shielding, shown in Figure 6, reveal a much more pronounced attenuation behavior. The rapid reduction in dose over a short distance reflects the strong shielding effectiveness of FeB-enhanced concrete. In this environment, the RF and GBR models clearly outperform the other approaches, with prediction curves that nearly coincide with the true dose points throughout the shielding thickness. Their ability to accurately model the sharp dose gradients near the source and the subsequent low-dose saturation regions underscores their robustness in highly nonlinear regimes.The shielding performance of FeB-enhanced concrete arises from the complementary physical roles of iron and boron. Boron provides a high neutron absorption cross section, particularly for thermal and epithermal neutrons, while the iron component, owing to its relatively high atomic number and density, plays a critical role in reducing the energy of fast neutrons through elastic and inelastic scattering interactions. This energy degradation shifts high-energy neutrons toward lower-energy regimes, creating favorable spectral conditions for efficient absorption by boron. The resulting multi-mechanism attenuation process leads to the complex, strongly nonlinear dose reduction observed within the concrete shielding.Consistent with this physical complexity, the KNN model exhibits reduced reliability in the shielding environment, where its locally driven structure limits its ability to produce stable attenuation curves in regions characterized by steep dose gradients. The LR model performs poorly, failing to capture the sharp dose decrease and deviating substantially from the true dose distribution. These observations confirm that log-linear LR modeling approaches are not suitable for describing neutron transport and shielding behavior in FeB-enhanced concrete.Overall, the results presented in Figures 5 and 6 demonstrate that RF and GBR models provide the most reliable and physically meaningful predictions for FeB-enhanced concrete, both in tunnel air and concrete shielding environments. These models consistently capture the complex, nonlinear, and multi-scale nature of neutron dose attenuation, whereas KNN offers only limited applicability and log-linear LR regression approaches prove inadequate for shielding analyses in high-energy proton accelerator facilities.The performance metrics of each model, along with their hyperparameter settings, R^2 values for the training and test sets, normalized RMSE (N-RMSE) results, and the number of samples used in the training and test sets, are summarized in Table 1. N-RMSE was calculated by normalizing the RMSE with respect to either the mean or the range of the data, allowing the error magnitude to be interpreted relative to both typical values and the spread of the dataset. The results indicate that model performance varies not only with the algorithm employed but also significantly depends on the environmental conditions and the type of shielding material.

Table 1. *Summary of machine learning model performance for each material-environment configuration.*

Material	Enviroment	Percent	Model	n	R2_test	NRMSE_test(%)	NMAE_test(%)
B_4C	Air	0.05	GBR	52	0.983 ± 0.012	3.14 ± 1.17	1.88 ± 0.84
B_4C	Air	0.05	KNN	52	0.950 ± 0.042	5.48 ± 3.37	3.14 ± 1.32
B_4C	Air	0.05	LRlog	52	0.854 ± 0.067	9.70 ± 3.94	6.37 ± 1.64
B_4C	Air	0.05	RF	52	0.991 ± 0.003	2.39 ± 0.78	1.47 ± 0.35
B_4C	Air	0.1	GBR	54	0.984 ± 0.009	3.16 ± 1.07	1.99 ± 0.68
B_4C	Air	0.1	KNN	54	0.960 ± 0.020	5.01 ± 1.62	2.96 ± 0.52
B_4C	Air	0.1	LRlog	54	0.856 ± 0.040	9.73 ± 2.49	6.73 ± 1.33
B_4C	Air	0.1	RF	54	0.989 ± 0.011	2.37 ± 1.37	1.53 ± 0.74
B_4C	Air	0.15	GBR	46	0.979 ± 0.008	3.53 ± 1.26	2.43 ± 0.76
B_4C	Air	0.15	KNN	46	0.935 ± 0.045	6.17 ± 3.35	3.81 ± 1.63
B_4C	Air	0.15	LRlog	46	0.875 ± 0.061	8.52 ± 3.83	5.86 ± 1.56
B_4C	Aİr	0.15	RF	46	0.987 ± 0.008	2.75 ± 1.32	1.86 ± 0.70
B_4C	Shield	0.05	GBR	137	0.992 ± 0.004	1.83 ± 0.78	0.73 ± 0.36
B_4C	Shield	0.05	KNN	137	0.977 ± 0.015	2.96 ± 1.51	0.97 ± 0.52
B_4C	Shield	0.05	LRlog	137	0.353 ± 0.090	16.06 ± 4.86	5.68 ± 2.73
B_4C	Shield	0.05	RF	137	0.996 ± 0.004	1.23 ± 0.61	0.45 ± 0.22
B_4C	Shield	0.1	GBR	127	0.991 ± 0.004	1.80 ± 0.70	0.80 ± 0.36
B_4C	Shield	0.1	KNN	127	0.971 ± 0.026	3.26 ± 2.44	1.10 ± 0.70
B_4C	Shield	0.1	LRlog	127	0.334 ± 0.091	16.11 ± 5.77	6.35 ± 3.03
B_4C	Shield	0.1	RF	127	0.996 ± 0.004	1.31 ± 0.84	0.53 ± 0.30
B_4C	Shield	0.15	GBR	126	0.990 ± 0.006	1.76 ± 0.42	0.75 ± 0.29
B_4C	Shield	0.15	KNN	126	0.973 ± 0.024	3.13 ± 2.23	0.98 ± 0.58
B_4C	Shield	0.15	LRlog	126	0.495 ± 0.080	14.18 ± 5.15	5.54 ± 2.67
B_4C	Shield	0.15	RF	126	0.994 ± 0.002	1.43 ± 0.48	0.56 ± 0.24
FeB	Air	0.05	GBR	49	0.977 ± 0.008	3.33 ± 1.33	2.18 ± 0.92
FeB	Air	0.05	KNN	49	0.938 ± 0.056	5.36 ± 3.80	3.19 ± 1.70
FeB	Air	0.05	LRlog	49	0.866 ± 0.066	7.81 ± 3.78	5.29 ± 1.23
FeB	Air	0.05	RF	49	0.985 ± 0.014	2.62 ± 1.67	1.54 ± 0.64
FeB	Air	0.1	GBR	51	0.984 ± 0.009	3.01 ± 0.90	1.90 ± 0.37
FeB	Air	0.1	KNN	51	0.944 ± 0.037	6.05 ± 3.59	3.10 ± 1.55
FeB	Air	0.1	LRlog	51	0.863 ± 0.057	9.58 ± 4.10	6.42 ± 1.90
FeB	Air	0.1	RF	51	0.988 ± 0.006	2.59 ± 0.66	1.67 ± 0.33
FeB	Air	0.15	GBR	49	0.966 ± 0.019	4.39 ± 2.19	2.82 ± 1.35
FeB	Air	0.15	KNN	49	0.947 ± 0.044	5.35 ± 3.56	3.42 ± 1.73
FeB	Air	0.15	LRlog	49	0.868 ± 0.049	8.26 ± 3.34	5.64 ± 1.31
FeB	Air	0.15	RF	49	0.976 ± 0.012	3.66 ± 1.88	2.27 ± 0.97
FeB	Shield	0.05	GBR	131	0.991 ± 0.004	1.81 ± 1.12	0.86 ± 0.53
FeB	Shield	0.05	KNN	131	0.977 ± 0.014	2.79 ± 1.86	1.02 ± 0.61
FeB	Shield	0.05	LRlog	131	0.457 ± 0.248	16.10 ± 8.41	7.20 ± 4.11
FeB	Shield	0.05	RF	131	0.990 ± 0.006	1.62 ± 0.93	0.68 ± 0.40
FeB	Shield	0.1	GBR	132	0.986 ± 0.008	1.96 ± 1.46	0.80 ± 0.58
FeB	Shield	0.1	KNN	132	0.967 ± 0.036	3.11 ± 2.78	1.05 ± 0.84
FeB	Shield	0.1	LRlog	132	0.366 ± 0.269	15.21 ± 8.14	6.00 ± 3.62
FeB	Shield	0.1	RF	132	0.992 ± 0.005	1.53 ± 1.15	0.59 ± 0.46
FeB	Shield	0.15	GBR	127	0.985 ± 0.008	2.14 ± 0.81	0.83 ± 0.41
FeB	Shield	0.15	KNN	127	0.964 ± 0.026	3.66 ± 2.32	1.23 ± 0.67
FeB	Shield	0.15	LRlog	127	0.318 ± 0.079	15.64 ± 5.82	5.82 ± 2.86
FeB	Shield	0.15	RF	127	0.992 ± 0.005	1.60 ± 0.82	0.57 ± 0.34

Table 1 summarizes the quantitative performance metrics of the machine learning models applied to B_4C- and FeB-enhanced concrete under different environmental conditions (tunnel air and concrete shielding). The table reports, for each model, the number of samples used (n), the coefficient of determination (R^2) on the test set, the normalized root mean square error (N-RMSE), and the normalized mean absolute error (NMAE). The N-RMSE values were obtained by normalizing the RMSE with respect to either the mean or the range of the dataset, allowing the prediction errors to be interpreted relative to both the characteristic magnitude and the variability of the data.

The results clearly indicate that model performance depends not only on the selected algorithm but also strongly on the environmental conditions and the type of shielding material. Overall, the RF and GBR models consistently exhibit the highest predictive accuracy across all configurations. These models achieve very high R^2 values—typically in the range of 0.98–0.996—together with low N-RMSE and NMAE values in both the tunnel air environment and the concrete shielding. This behavior demonstrates

the strong capability of tree-based ensemble methods to capture the nonlinear, multi-scale attenuation characteristics of secondary neutron dose distributions.

The KNN model provides acceptable performance, particularly in the tunnel air environment; however, it generally yields higher error metrics than RF and GBR. This relative degradation becomes more pronounced in the shielding environment, where steep dose gradients and highly heterogeneous attenuation behavior are present. Such sensitivity can be attributed to the local, instance-based nature of KNN and its limited generalization capability in complex, high-gradient data spaces.

In contrast, the log-linear LR model exhibits markedly poorer performance, especially within the concrete shielding. For both B_4C- and FeB-enhanced concretes in the shielded environment, log-linear LR is characterized by very low R^2 values (approximately 0.3–0.5) and high N-RMSE values reaching up to 14-16%. These results indicate that the sharp and strongly nonlinear dose attenuation observed within shielding materials cannot be adequately represented by simple log-linear formulations. Although log-linear LR performs comparatively better in the tunnel air environment, it still remains clearly inferior to the nonlinear machine learning approaches.

From a material-specific perspective, similar performance trends are observed for both B_4C- and FeB-enhanced concretes. However, the FeB-based shielding configurations exhibit slightly more complex attenuation behavior, particularly in the shielded environment, due to the combined effects of iron-induced neutron scattering and boron-based absorption. This increased physical complexity further challenges linear modeling approaches, while RF and GBR remain robust and accurate across all FeB configurations.In summary, the performance metrics presented in Table 1 demonstrate that nonlinear machine learning models provide a reliable and physically consistent framework for predicting secondary neutron dose distributions in both tunnel air and concrete shielding environments. Among the evaluated approaches, RF and GBR emerge as the most effective and stable models across varying material compositions and environmental conditions. Conversely, the limited predictive capability of the log-linear regression approach highlights its unsuitability for neutron transport and shielding problems in high-energy proton accelerator facilities. To further investigate the learning behavior and error characteristics of the models, the spatial variation of prediction errors was analyzed using the root mean square error (RMSE) metric. Rather than relying solely on global performance indicators, evaluating the distance-dependent variation of RMSE enables a detailed assessment of model accuracy and stability in both the near-field and far-field regions. In this context, distance-dependent test RMSE profiles derived from 5-fold cross-validation were examined.

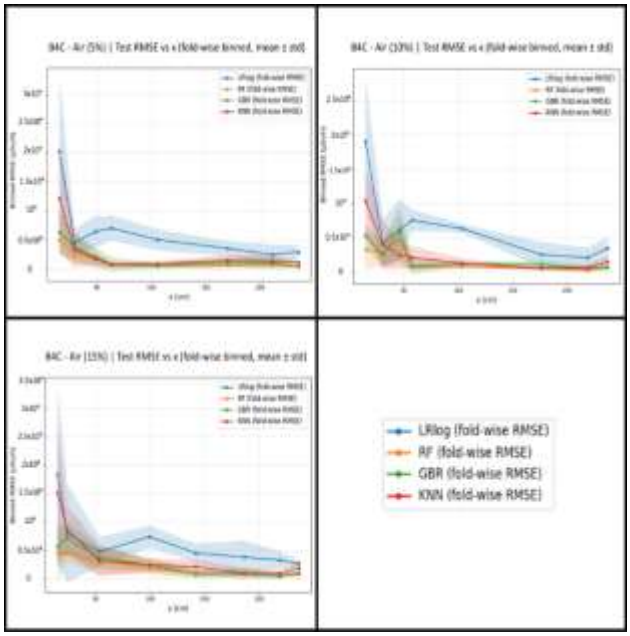

Figure 7*. Distance-dependent variation of test RMSE as a function of xfor B_4C-enhanced concrete with 5%, 10%, and 15% boron content in the tunnel air environment. Results are presented as mean ± standard deviation based on 5-fold cross-validation for the log-linear LR, RF, GBR, and KNN models.*

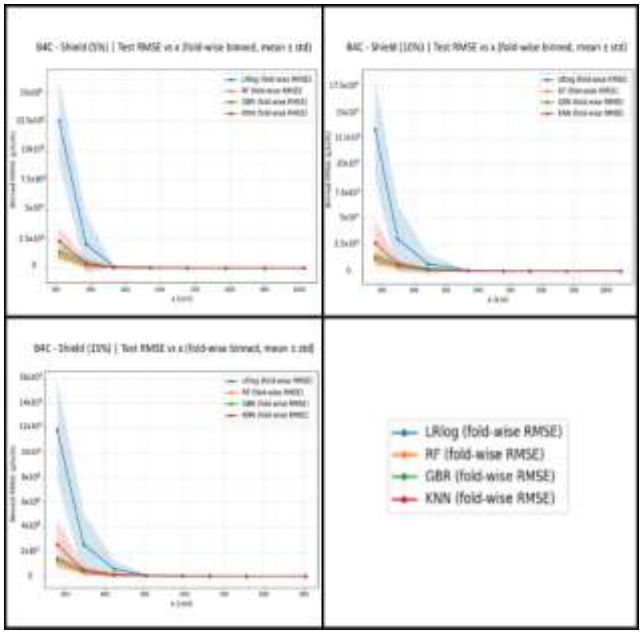

Figure 8*. Distance-dependent variation of test RMSE as a function of xfor B_4C-enhanced concrete with 5%, 10%, and 15% boron content in the concrete shielding environment. Results are presented as mean ± standard deviation based on 5-fold cross-validation for the log-linear LR, RF, GBR, and KNN models.*

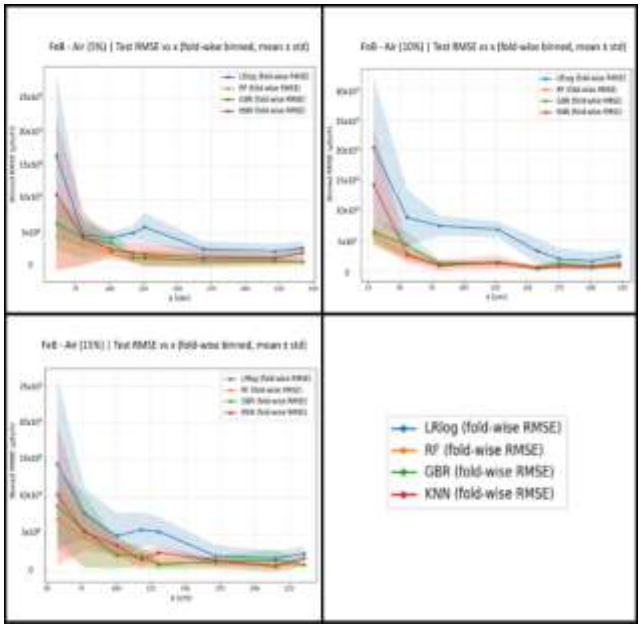

Figure 9. *Distance-dependent variation of test RMSE as a function of xfor FeB-enhanced concrete with 5%, 10%, and 15% additive content in the tunnel air environment. Results are presented as mean ± standard deviation based on 5-fold cross-validation for the log-linear LR, RF, GBR, and KNN models.*

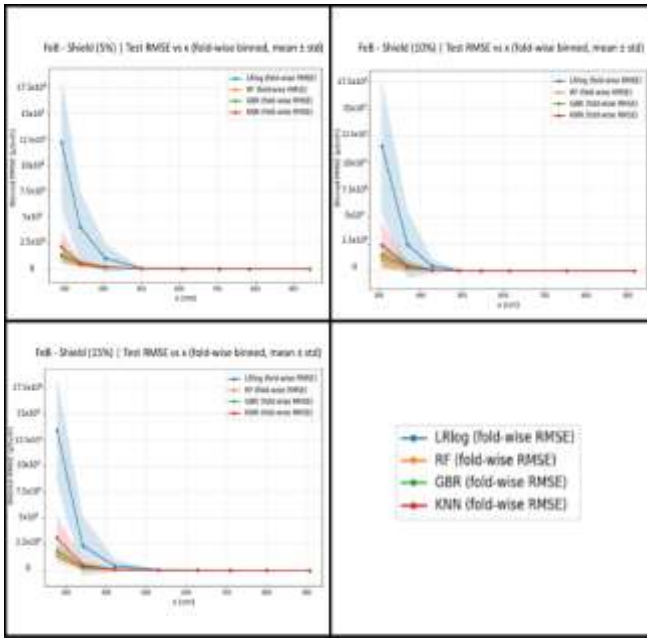

Figure 10. *Distance-dependent variation of test RMSE as a function of xfor FeB-enhanced concrete with 5%, 10%, and 15% additive content in the concrete shielding environment. Results are presented as mean ± standard deviation based on 5-fold cross-validation for the log-linear LR, RF, GBR, and KNN models.*

For B_4C-enhanced concrete, the RMSE profiles obtained in the tunnel air environment (Figure 7) indicate that all models exhibit their highest error levels in the near-field region close to the source. This behavior is associated with the presence of steep spatial dose gradients and the strongly nonlinear nature of the underlying physical processes. As the distance from the source increases, RMSE values decrease systematically, reflecting improved prediction accuracy in the far-field regime. Among the evaluated models, Random Forest (RF) and Gradient Boosting Regressor (GBR) consistently achieve lower RMSE values across the entire distance range and display narrower uncertainty bands, indicating stable and robust learning behavior. In contrast, the KNN model shows noticeable fluctuations, particularly at intermediate distances, while the log-linear LR model exhibits persistently higher and more variable RMSE values, highlighting its limited capability to capture nonlinear dose–distance relationships.

The RMSE profiles for B_4C-enhanced concrete in the shielding environment (Figure 8) reveal an even stronger dependence on distance. Extremely high RMSE values are observed in the immediate vicinity of the source due to the sharp dose attenuation within the concrete shield. Beyond this near-field region, however, RF and GBR rapidly suppress the prediction error, converging to near-zero RMSE values and maintaining this performance over a wide distance range. This behavior demonstrates that these models successfully learn the dominant nonlinear attenuation mechanisms governing neutron transport within the shielding material. In contrast, KNN exhibits reduced stability in the near-field, while LR fails to represent the steep dose gradients, resulting in elevated RMSE levels over a broader spatial range.

The distance-dependent RMSE profiles obtained for FeB-enhanced concrete (Figures 9 and 10) show trends that are largely consistent with those observed for B_4C. In the tunnel air environment (Figure 9), the highest RMSE values again occur near the source, followed by a gradual reduction with increasing distance. RF and GBR models demonstrate superior performance, characterized by lower RMSE values and reduced fold-to-fold variability across all distances. The KNN model exhibits pronounced fluctuations at intermediate distances, whereas the LR model consistently yields higher RMSE values, indicating insufficient generalization even in the air environment.

In the shielding environment for FeB-enhanced concrete (Figure 10), the prediction task becomes more challenging due to the combined effects of iron-induced neutron scattering and boron-based absorption. These multi-mechanism attenuation processes lead to extremely steep dose gradients in the near-field region, resulting in high RMSE values close to the source. Despite this complexity, RF and GBR models rapidly reduce RMSE beyond the initial shielding thickness and maintain very low and stable error levels in the far-field region. This outcome confirms their ability to capture the

strongly nonlinear and multi-scale attenuation behavior characteristic of FeB-enhanced concrete. Conversely, KNN shows limited robustness near the source, and LR remains unable to reproduce the rapid dose attenuation, leading to persistently higher RMSE values.Overall, the distance-dependent RMSE analyses presented in Figures 7-10 clearly demonstrate that model performance is strongly distance-dependent, with the most challenging prediction region located in the near-field where dose gradients are steepest. Across all material and environmental configurations, Random Forest and Gradient Boosting Regressor models consistently provide the lowest prediction errors and the highest spatial stability in both near-field and far-field regimes. In contrast, KNN offers limited reliability, and log-linear regression approaches are inadequate for representing the complex spatial behavior of secondary neutron dose attenuation in both B_4C- and FeB-enhanced concrete shielding systems. Radiation has been studied in a variety of different purposes and reported in the literature [41-60].

4. Conclusions

In this study, a hybrid MC-ML framework was developed to model the secondary neutron dose distributions generated by the interaction of 1000 MeV protons with a copper target. Neutron dose data obtained from FLUKA simulations were evaluated for both tunnel air and concrete shielding environments using B_4C- and FeB-enhanced concrete at additive fractions of 5%, 10%, and 15%. Within this framework, log-linear LR, KNN, RF, and GBR models were systematically trained and tested.

The results demonstrate that neutron dose attenuation exhibits a strongly nonlinear and distance-dependent behavior, particularly within shielding materials where steep dose gradients occur over short spatial ranges. In addition to global performance metrics, distance-dependent RMSE analyses revealed pronounced differences in model accuracy between the near-field and far-field regions. Across all material compositions and environmental configurations, RF and GBR models consistently outperformed log-linear LR and KNN, providing superior predictive accuracy and spatial stability. In contrast, the log-linear LR model failed to adequately represent the nonlinear dose–distance relationship, while KNN showed limited robustness, especially in regions characterized by sharp attenuation.

Comparative analyses of B_4C- and FeB-enhanced concretes indicate that both materials provide effective neutron shielding; however, FeB-enhanced concrete exhibits more complex attenuation behavior due to the synergistic physical roles of iron and boron. Iron contributes to fast-neutron energy degradation through elastic and inelastic scattering, while boron provides efficient absorption at lower neutron energies. This multi-mechanism shielding behavior results in highly nonlinear dose distributions, which can be reliably captured only by advanced nonlinear machine learning models. Distance-dependent error analyses further show that prediction uncertainty is highest near the source and rapidly decreases beyond the initial shielding thickness when RF and GBR models are employed.

Overall, this study demonstrates that nonlinear, tree-based machine learning models trained on MC simulation data offer a reliable, rapid, and computationally efficient alternative for neutron dose estimation and shielding analysis in high-energy proton accelerator facilities. The proposed framework enables accurate dose prediction across different shielding materials, additive fractions, and spatial regions, thereby providing a powerful tool for shielding design optimization and radiation safety assessments. Future work will focus on extending this approach to three-dimensional geometries, additional energy ranges, and real-time surrogate modeling for accelerator operation and facility design.

Author Statements:

- **Ethical approval:** The conducted research is not related to either human or animal use.
- **Conflict of interest:** The authors declare that they have no known competing financial interests or personal relationships that could have appeared to influence the work reported in this paper
- **Acknowledgement:** The numerical calculations reported in this paper were performed at TUBITAK ULAKBIM, High Performance and Grid Computing Center (TRUBA Resources).
- **Author contributions:** The authors declare that they have equal right on this paper.
- **Funding information:** The authors declare that there is no funding to be acknowledged.
- **Data availability statement:** The data that support the findings of this study are available on request from the corresponding author. The data are not publicly available due to privacy or ethical restrictions.

References

[1] Sarıyer, D., 2025. FLUKA Monte Carlo assessment of Fe_2B-based shielding materials for secondary neutrons in a 1000 MeV proton accelerator. *International Journal of Computational and*

Experimental Science and Engineering, **11**(4), 9864–9869. https://doi.org/10.22399/ijcesen.4544

[2] Shittu, R.A., Alhamadi, F., Sherief, M., AlFantazi, A., Alkaabi, A.K., 2025. Factors influencing the radiation shielding capacity of concrete exposed to aggressive arid environment: A comprehensive review. *International Journal of Concrete Structures and Materials*, **19**, 91. https://doi.org/10.1186/s40069-025-00817-w

[3] Hartling, K., Yamani, Z., Harrison, G., Ha, H., Ali, F., Anghel, V., 2025. A simulation study of neutron transmission and secondary neutron generation in lithium and boron-based shielding materials. *Advances in Space Research*. https://doi.org/10.1016/j.asr.2025.12.039

[4] Maldarreh, R.B., Saleh, A., Lotfiaghah, A., Tajidine, S.M., Mansour, F.E., Zakaly, H.M.H., 2025. Achieving synergistic neutron–gamma shielding in G5 composite (65Al–15SiC–20TiC): Density functional performance via Monte Carlo modeling. *Applied Radiation and Isotopes*, **229**, 113553. https://doi.org/10.1016/j.apradiso.2025.113553

[5] Barbhuiya, S., Das, B.B., Norman, P., Qureshi, T., 2024. A comprehensive review of radiation shielding concrete: Properties, design, evaluation, and applications. *Structural Concrete*. https://doi.org/10.1002/suco.202400519

[6] El-Khayatt, A.M., Akkurt, I., 2013. Photon interaction, energy absorption and neutron removal cross section of concrete including boron and iron additives. *Annals of Nuclear Energy*, **60**, 8–14. https://doi.org/10.1016/j.anucene.2013.04.029

[7] Sarıyer, D., Küçer, R., & Küçer, N., 2015. Neutron shielding properties of concretes containing boron carbide and ferro-boron. *Procedia – Social and Behavioral Sciences, 195*, 1752-1756. https://doi.org/10.1016/j.sbspro.2015.06.320

[8] Sarıyer, D., A FLUKA-based study on the effect of boron-enhanced concrete on secondary neutron dose under proton beam loss scenarios, *International Journal of Natural-Applied Sciences and Engineering* **3**(1) (2025) 113–119. https://doi.org/10.22399/ijnasen.30

[9] Sarıyer, D., Küçer, R., Küçer, N., 2015. Neutron Shielding Properties of Concrete and Ferro - Boron. ACTA PHYSICA POLONICA A., 127 (2 - B), 201 - 202.

[10] Sarıyer, D., Küçer, R., Küçer, N., 2015. Neutron Shielding Properties of Concretes Containing Boron Carbide and Ferro - Boron. Elsevier Procedia Social and Behavioral Sciences. 195, 1752 - 1756.

[11] Paul, M. B., Dutta Ankan, A., Deb, H., & Ahasan, M. M., 2023. A Monte Carlo simulation model to determine the effective concrete materials for fast neutron shielding. *Radiation Physics and Chemistry, 202*, 110476. https://doi.org/10.1016/j.radphyschem.2022.110476

[12] Sarıyer, D., 2020. *Investigation of Neutron Attenuation through FeB, Fe_2B and Concrete*. Acta Physica Polonica A, 137(4), 539-542. https://doi.org/10.12693/APhysPolA.137.539

[13] S. H. Rokni, S. H., Cossairt, J. D., Liu, J. C. *Radiation Shielding at High-Energy Electron and Proton Accelerators*, Stanford Linear Accelerator Center, 10 December 2007.

[14] Jayaraj, V.V., Padmaprabu, C., Ojha, B.K., Dash, B.S., Padalakshmi, M., Anandaraj, V., Vijay Kumar, R., Vijayaragavan, A., Venkiteswaran, C.N., Karthik, V., Divakar, R., 2021. Irradiation behaviour of ferroboron – An alternate in-core shielding material for sodium-cooled fast reactors. *Nuclear Engineering and Design*, 377, 111126. https://doi.org/10.1016/j.nucengdes.2021.111126

[15] Hançerlioğulları, A., 2006. Monte Carlo simulation method and MCNP code system. *Kastamonu Education Journal*, 14(2), 545–556.

[16] A. J. Jinia, S. D. Clarke, J. M. Moran and S. A. Pozzi, "Intelligent Radiation: A review of Machine learning applications in nuclear and radiological sciences", Annals of Nuclear Energy, 201, 110444, 2024, https://doi.org/10.1016/j.anucene.2024.110444

[17] Chen, L. F., 2025. Machine learning-assisted optimization of modular neutron shielding based on Monte Carlo simulations, *arXiv preprint*, arXiv:2504.12345, 24 Nisan 2025; son revizyon: 26 Mayıs 2025. https://arxiv.org/abs/2504.12345

[18] Alghamdi, A. A. A., 2024. Machine learning for predicting neutron effective dose". Applied Sciences, 14(13), 5740,. https://doi.org/10.3390/app14135740

[19] Marcato, D., 2023. *Intelligent Control Systems and Machine Learning Approaches for Particle Accelerators*. Ph.D. Thesis, Department of Information Engineering, University of Padova, Italy.

[20] Nahool, T. A., Abdelmonem, A. M., Ali, M. S. and Yasser, A. M. 2024. Using machine learning to predict gamma shielding properties: a comparative study, *New Journal of Physics*, cilt 26, s. 093035. https://doi.org/10.1088/1367-2630/ad4a21

[21] Jinia, A. J., Clarke, S. D., Moran, J. M., Pozzi, S. A., 2024. Intelligent Radiation: A review of Machine Learning applications in nuclear and radiological sciences, *Annals of Nuclear Energy*, vol. 201, 110444. Available online: February 28, 2024. DOI: https://doi.org/10.1016/j.anucene.2024.110444

[22] Edelen, A. L., Biedron, S. G., Chase, B. E., Edstrom Jr., D., Milton, S. V. and Stabile, P., 2016. Neural Networks for Modeling and Control of Particle Accelerators, *IEEE Transactions on Nuclear Science*, vol. 63, no. 2, pp. 878–897, Apr. 2016. doi: 10.1109/TNS.2016.2521598

[23] Chowdhury, R.P., Zamora, J., Ginter, T., Bollen, G., 2025. Machine learning in accelerator shielding: Application using convolutional neural networks. *Transactions of the American Nuclear Society*. https://doi.org/10.13182/T131-4592

[24] Pal Chowdhury, R., Zamora, J.C., Bollen, G., Ginter, T., 2026, *Surrogate modeling of Monte Carlo radiation transport with convolutional neural networks for shielding optimization*, Nuclear Instruments and Methods in Physics Research B **570**, 165909. https://doi.org/10.1016/j.nimb.2025.165909

[25] Puppala, A., 2025. A comprehensive review of linear regression models: Theory, applications, and advanced techniques. *International Journal of Machine Learning and Cybernetics (IJMLC)*, 3(1), 1-6. https://doi.org/10.34218/IJMLC_03_01_001

[26] Sarkar, A., Kashikar, P., 2024. *Literature review of implementation of machine learning algorithms for improving the network security*. International Journal of Science Academic Research **5** (1), 6915-6922.

[27] Alkharisi, M.K., Dahish, H.A., Youssf, O., 2024, *Prediction models for the hybrid effect of nano materials on radiation shielding properties of concrete exposed to elevated temperatures*, Case Studies in Construction Materials **21**, e03750. https://doi.org/10.1016/j.cscm.2024.e03750

[28] Shen, J., 2017. *Log-linear regression*, in: Encyclopedia of Database Systems, Springer, New York, USA. https://doi.org/10.1007/978-1-4899-7993-3_543-2

[29] Benoit, K., 2011. *Linear regression models with logarithmic transformations*, Lecture Notes, London School of Economics and Political Science, London, UK.

[30] Pandey, D., Niwaria, K., & Chourasia, B., 2019. Machine Learning Algorithms: A Review. *International Research Journal of Engineering and Technology (IRJET)*, 6(2), 916. ISSN: 2395-0056 (e-ISSN), 2395-0072 (p-ISSN).

[31] Khatiwada, A., Klasky, M., Lombardi, M., Matheny, J., & Mohan, A., 2023. Machine learning technique for isotopic determination of radioisotopes using HPGe γ-ray spectra. *Nuclear Instruments and Methods in Physics Research Section A: Accelerators, Spectrometers, Detectors and Associated Equipment*, 1046, 168409. https://doi.org/10.1016/j.nima.2023.16840

[32] Rodriguez, S.A., Cho, J., Goes, C.R., Kim, Y., Kim, Y., Lee, S., Yeon, J., 2025. *A feasibility study on gradient boosting regressor for subsurface sensor-based surface instability assessment*, Land, 14, 565. https://doi.org/10.3390/land1403056

[33] Natekin, A., Knoll, A., 2013, *Gradient boosting machines: A tutorial*, Frontiers in Neurorobotics **7**, Article 21. https://doi.org/10.3389/fnbot.2013.00021

[34] Singh, U., Rizwan, M., Alaraj, M., Alsaidan, I., 2021, *A machine learning-based gradient boosting regression approach for wind power production forecasting: A step towards smart grid environments*, Energies **14**, 5196. https://doi.org/10.3390/en14165196

[35] Kotsiantis , S.B., 2007. Supervised machine learning: A review of classification techniques, Informatica 31, 249-268.

[36] Islam, M.J., Wu, Q.M.J., Ahmadi, M., Sid-Ahmed, M.A., 2010, *Investigating the performance of Naïve Bayes classifiers and K-nearest neighbor classifiers*, Journal of Convergence Information Technology **5**(2), 1-10. https://doi.org/10.4156/jcit.vol5.issue2.15

[37] Anunike, G., Tarabin, M., Hisseine, O., 2025, *Machine learning–supported prediction of the radiation-shielding efficiency of ultra-high-performance concrete*, Full Paper Transactions, SMiRT 28, Toronto, Canada, August 10-15.

[38] Lattimer, B. Y., Hodges, J. L., & Lattimer, A. M., 2020. Using machine learning in physics-based simulation of fire. *Fire Safety Journal*, 114, 102991. https://doi.org/10.1016/j.firesaf.2020.102991

[39] Pandey, D., Niwaria, K., & Chourasia, B., 2019. Machine Learning Algorithms: A Review. *International Research Journal of Engineering and Technology (IRJET)*, 6(2), 916. ISSN: 2395-0056 (e-ISSN), 2395-0072 (p-ISSN)

[40] Salazar, J. J., Garland, L., Ochoa, J., & Pyrcz, M. J.,2022. Fair train-test split in machine learning: Mitigating spatial autocorrelation for improved prediction accuracy. *Journal of Petroleum Science and Engineering*, 209, 109885. https://doi.org/10.1016/j.petrol.2021.109885

[41]Şerife Evrim ARICI, Aslı KARA, Kadir GÜNOĞLU, & İskender AKKURT. (2016). Effects of Different Gamma Ray Doses on In Vitro Potato Production. *International Journal of Natural-Applied Sciences and Engineering*, *1*(1). https://doi.org/10.22399/ijnasen.3

[42]Soyal, H., & Sarıhan, M. (2025). The Place, Importance and Development Approaches of Radiation Safety and Protection Education in Associate Degree Health Programs. *International Journal of Sustainable Science and Technology*, *3*(1). https://doi.org/10.22399/ijsusat.11

[43]Betul Cetin, & Betul Sezer. (2025). Comparison of the radiation shielding effect of travertine and gasconcrete. *International Journal of Natural-Applied Sciences and Engineering*, *3*(1). https://doi.org/10.22399/ijnasen.31

[44]Soyal, H., & Canpolat, M. (2025). Intersections of Ergonomics and Radiation Safety in Interventional Radiology. *International Journal of Sustainable Science and Technology*, *3*(1). https://doi.org/10.22399/ijsusat.12

[45]Sibel ÖZAVCI, & Betül ÇETİN. (2017). Experimental Investigation of Radiation Shielding Effect in Different Doped Slag Concrete. *International Journal of Sustainable Science and Technology*, *2*(1). https://doi.org/10.22399/ijsusat.23

[46]García, R. (2025). Optimization in the Geometric Design of Solar Collectors Using Generative AI Models (GANs). *International Journal of Applied Sciences and Radiation Research* , *2*(1). https://doi.org/10.22399/ijasrar.32

[47]Betul Cetin, Arzu Poyraz, & Melek Gul. (2026). Examination of the radiation absorption parameters of CuO coatings prepared at different ratios. *International Journal of Sustainable Science and Technology*, *4*(1). https://doi.org/10.22399/ijsusat.35

[48]Morad Kh. Hamad. (2025). Synergistic Evaluation of Ionizing Radiation Shielding in Novel Lead-Free Alloys Using Geant4 MC toolkit. *International*

Journal of Applied Sciences and Radiation Research , *2*(1). https://doi.org/10.22399/ijasrar.47

[49]Sağlam, F., & Cetin, B. (2025). Investigation of Gamma Shielding Properties of Some Industrial Materials. *International Journal of Computational and Experimental Science and Engineering*, *11*(2). https://doi.org/10.22399/ijcesen.1357

[50]Nuray Kutu. (2026). Radiation Shielding Properties of recycled waste glass color doped powder cement pastes. *International Journal of Applied Sciences and Radiation Research* , *3*(1). https://doi.org/10.22399/ijasrar.55

[51]AYDIN, H., SÜSOY DOĞAN, G., TEKİN, H. O., ŞEN BAYKAL, D., & İLTUŞ, Y. C. (2025). Examining the Neutron and Gamma Attenuation Characteristics of Various Amorphous Structures with Bioactive Properties. *International Journal of Computational and Experimental Science and Engineering*, *11*(3). https://doi.org/10.22399/ijcesen.2176

[52]Günoğlu, K., & Akkurt, İskender. (2023). Gamma-ray attenuation properties carbide compounds (WC, Mo2C, TiC, SiC, B4C) using Phy-X/PSD software. *International Journal of Applied Sciences and Radiation Research* , *1*(1), 1–8. https://doi.org/10.22399/ijasrar.6

[53]Soyal, H., & Sarıhan, M. (2025). Evaluation of Radiation Protection Knowledge and Attitudes of Health Services Vocational School Students Participating in Practice in Radiated Environments. *International Journal of Computational and Experimental Science and Engineering*, *11*(2). https://doi.org/10.22399/ijcesen.508

[54]Waheed, F., Mohamed Abdulhusein Mohsin Al-Sudani, & Iskender Akkurt. (2025). The Experimental Enhancing of the Radiation Shield Properties of Some Produced Compounds. *International Journal of Applied Sciences and Radiation Research* , *2*(1). https://doi.org/10.22399/ijasrar.1

[55]Emikönel, S., & Akkurt, İskender. (2025). Radiation Shielding Properties of B2O3-Bi2O3 Glass . *International Journal of Computational and Experimental Science and Engineering*, *11*(2). https://doi.org/10.22399/ijcesen.2157

[56]Abuş, F., Gürçalar , A., Günay, O., Tunçman , D., Kesmezacar, F. F., & Demir, M. (2024). Determination of Radiation Dose Levels Incurred by Lenses During Scopy Imaging. *International Journal of Applied Sciences and Radiation Research* , *1*(1). https://doi.org/10.22399/ijasrar.11

[57]Hussein Majid, & Mawada M. Funjan. (2025). Comparison of radiation dose parameters between LDCT and SDCT in pediatric brain CT Protocols. *International Journal of Computational and Experimental Science and Engineering*, *11*(3). https://doi.org/10.22399/ijcesen.3431

[58]Özlen, M. S., Cuma, A. B., Yazıcı, S. D., Yeğin, N., Demir, Özge, Aksoy, H., … Günay, O. (2024). Determination of Radiation Dose Level Exposed to Thyroid in C-Arm Scopy. *International Journal of Applied Sciences and Radiation Research* , *1*(1). https://doi.org/10.22399/ijasrar.13

[59]Nasser Khidhr Alhazmi, Sultan Dagham Alanazi, Hammad Shabeeb A Alrowily, Khaled Fayez Alkhamsan, Fawaz Awad Dahisan Al-Rashidi, Al-Salem Sultan Mohammed, … Ahmed Ayyaf k AlQusayri. (2026). Radiation Safety Compliance and Protective Practices Among Radiologic Technologists. *International Journal of Computational and Experimental Science and Engineering*, *10*(4). https://doi.org/10.22399/ijcesen.4664

[60]Vural, M., Kabaca, A., Aksoy, S. H., Demir, M., Karaçam, S. Çavdar, Ulusoy, İdil, … Günay, O. (2025). Determination Of Radiation Dose Levels to Which Partois And Spinal Cord (C1-C2) Regions Are Exposed In Computed Tomography Brain Imaging. *International Journal of Applied Sciences and Radiation Research* , *2*(1). https://doi.org/10.22399/ijasrar.17